Geothermics 84 (2020) 101743

Contents lists available at ScienceDirect

Geothermics

journal homepage: www.elsevier.com/locate/geothermics

Seismic exploration survey northeast of the Tres Virgenes Geothermal Field, Baja California Sur, Mexico: A new Geothermal prospect

E.B. Sena-Lozoya[a], M. González-Escobar[b,*], E. Gómez-Arias[c], A. González-Fernández[b], M. Gómez-Ávila[d]

[a] Posgrado en Ciencias de la Tierra, Centro de Investigación Científica y de Educación Superior de Ensenada, Ensenada, BC, 22860, Mexico
[b] Centro de Investigación Científica y de Educación Superior de Ensenada, Ensenada, BC, 22860, Mexico
[c] CONACYT - Centro de Investigación Científica y de Educación Superior de Ensenada, Ensenada, BC, 22860, Mexico
[d] Instituto de Ingeniería y Tecnología, Universidad Autónoma de Ciudad Juárez, Ciudad Juárez, Chihuahua, 32310, Mexico

ARTICLE INFO

Keywords:
Las Tres Vírgenes volcanic complex
La Reforma caldera
Geothermal exploration
MASW
Seismic reflection

ABSTRACT

Geophysical prospecting has become essential to identify low enthalpy areas with geothermal potential, mainly, for direct uses. The present study uses two seismic techniques and lithological information from shallow boreholes located northeast of the Tres Virgenes Geothermal Field, B.C.S., Mexico, to identify geological structures of geothermal interesting. Using the Multichannel Analysis of Surface Waves method (MASW), it was possible to correlate the S-wave velocity model with the lithology from two wells drilled over the seismic profile. Additionally, we generated a seismic reflection model to describe the geological distribution of deeper structures. The reflection profile, which reached depths of about 500 m, was complemented with superficial information from a MASW velocity model. We found a relationship between the velocity distribution of P and S waves from both models. The integration of seismic and lithological information allows us to identify a very fractured subsurface and a deep zone with possible geothermal interest.

1. Introduction

In recent years, seismic prospecting has been widely used for subsoil characterization in many applications. Although seismic refraction and reflection methods, as well as surface waves analysis, share the same theoretical basis, each one is distinguished because the parameters analyzed yield in particular geological features information. Therefore, the methodology to be used will depend on the objective of the study, and it is important to consider the limitations of each technique. For example, the seismic refraction method does not allow to identify low-velocity zones in depth (Sheriff and Geldart, 1995).

The seismic reflection is one of the most utilized geophysical exploration techniques since it allows to identify seismic stratigraphic and structural details from subsurface images at scales from tens to thousands of meters (Kearey et al., 2002). It has been recently implemented worldwide as an auxiliary tool for geothermal exploration (Manzella, 1973; Lamarche, 1992; Liotta and Ranalli, 1999; Cameli et al., 2000; Brogi et al., 2003; Bruno et al., 2003; Zollo et al., 2008; Liberty et al., 2015, among others). In this sense, seismic reflection is mainly used for characterization of faults related to hydrothermal fluids transport and other structures associated with the geothermic play, like fluids accumulation, hydrothermal vents, intrusive bodies that work as heat sources such as sills and dikes, and fronts of thermal alteration (MØller Hansen, 2006; Kluesner, 2011; Lizarralde et al., 2011; Planke et al., 2015; Sahakian et al., 2016; Gallegos-Castillo, 2019).

The seismic reflection method has represented a challenge when it is applied in volcanic areas due to high attenuation of seismic energy in depth, caused because the high-density of volcanic rocks generate that most of the seismic energy is reflected towards the surface letting just a small amount to be transmitted to greater depths, and, therefore, a low quality of information beneath is received (Bruno et al., 2003; Liberty et al., 2015). However, considering that many of the geothermal prospects are located in volcanic zones, either near-surface or at a great depth, techniques have been implemented to improve the quality of the resulting images, as well as the integration of different geophysical methods and borehole data that complement the seismic results (Planke and Eldholm, 1999; Bruno and Castiello, 2009; Liberty et al., 2015).

On the other hand, Multichannel Analysis of Surface Waves (MASW) is one of the most used methods in geotechnical characterization of near-surface subsurface materials (Park, 2001). This technique allows the generation of V_S *vs* Z models (S- or shear-wave velocity *vs* depth), from spectral analysis of surface waves. It is also used to identify

* Corresponding author.
E-mail address: mgonzale@cicese.mx (M. González-Escobar).

https://doi.org/10.1016/j.geothermics.2019.101743
Received 17 July 2019; Received in revised form 1 October 2019; Accepted 21 October 2019
Available online 11 November 2019
0375-6505/ © 2019 Elsevier Ltd. All rights reserved.

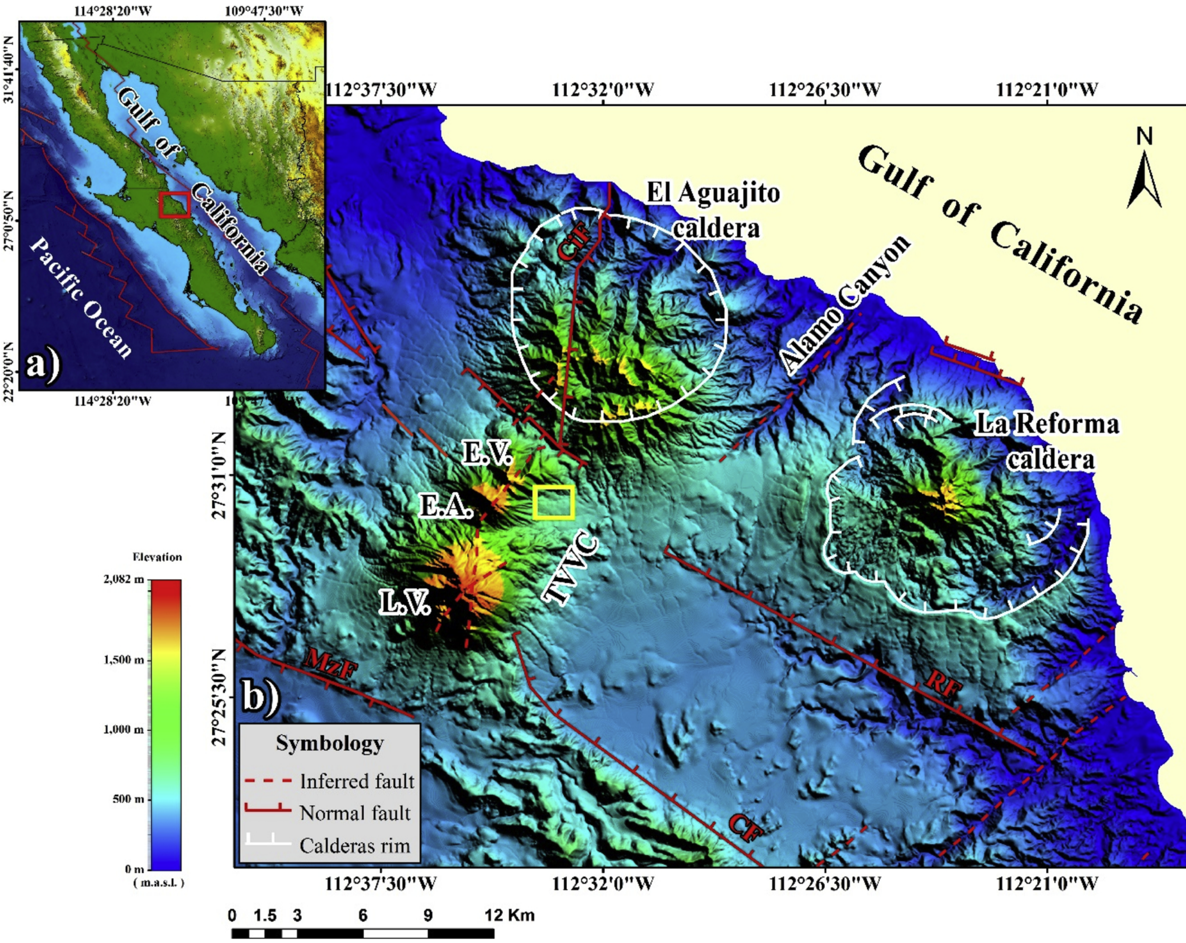

Fig. 1. a) Location of the Quaternary volcanoes in central Baja California, Mexico (red box). b) Main structures are: System of aligned volcanoes Las Tres Vírgenes (TVVC): La Virgen (L.V.), El Azufre (E.A.) and El Viejo (E.V.); Las Tres Vírgenes geothermal field (LTVGF; yellow box); and El Aguajito and La Reforma calderas, both limited by the Alamo Canyon. Main normal faults: RF (Reforma), CF (Campamento), CiF (Cimarrón), MzF (Mezquital). Regional faults and calderas boundaries were taken from Avellán et al. (2018). DEM taken from INEGI (2019).

tunnels or caves, to determine soil movement during large earthquakes, soil amplification and liquefaction factor, in the characterization of unconsolidated sediments, to map surface faults buried by sediments and to delimit the top of the basement, as well as to complement information provided by other geophysical methodologies (Park et al., 1998, 1999; Xia et al., 1999; Lin et al., 2004; Orfanos and Apostolopoulos, 2012; Almalki and Munir, 2013; Roy and Jakka, 2017). The MASW method is mainly used in areas of sedimentary environment and has provided reliable S-wave values compared to borehole V_S measurements (Xia et al., 1999, 2000; Stephenson et al., 2005; Ismail et al., 2014). Thus we can expect good responses when applied in volcanic regions. Few studies report the resolution and effectiveness of this method in volcanic environments near areas with geothermal potential (Sena-Lozoya, 2019). Furthermore, Sáez Blázquez et al. (2018) used the MASW (V_S) and seismic refraction (V_P) methods as support in estimating thermal conductivity (k) of rocks from a geothermal zone of low enthalpy, obtaining a good relationship between V_S, V_P y k.

The MASW method can usually achieve maximum depths of ~ 30 m, considering a sled hammer as a seismic source, while seismic reflection can visualize hundreds to thousands of meters, with a lack of resolution in the first meters of depth. Therefore, complementing the results of both techniques can be very useful in understanding both superficial and in-depth information on the study area.

In this work, we carried out an acquisition of 4.8 km of MASW and 2.2 km of seismic reflection data southwest the La Reforma caldera, close to the boundary with the Las Tres Vírgenes geothermal field, Baja California Sur (BCS), Mexico. 2D seismic models were generated with both methods (MASW and reflection). Also, two boreholes of 55 m depths were drilled (along of the seismic profile), and geological cores were recovered to reconstruct the lithological profile for each well and were used as geological referents of the subsurface to validate 2D seismic models. The main objective of this work is for the first time to understand the distribution of the shallow geological structures under the La Reforma caldera and to identify seismic features related to low-enthalpy thermal activity, for a new geothermal prospect.

2. Geological synthesis

Tres Virgenes volcanic complex is located in the northeastern part of Baja California Sur, Mexico, about 35km NW from Santa Rosalía city (Fig. 1). This complex is situated within the transtensional tectonic domain (*pull-apart*) of the fault system with a right lateral displacement that caused the separation of the Baja California peninsula from western Mexico (Garduño-Monroy et al., 1993). The region comprises three Quaternary volcanic structures (Garduño-Monroy et al., 1993; López-Hernández et al., 1995; Macías Vázquez and Jiménez Salgado, 2013; Avellán et al., 2018) that from older to younger are: La Reforma caldera (LRC; 1.38 ± 0.03 Ma; García Sánchez et al., 2019; Schmitt et al., 2006); El Aguajito caldera (EAC; 1.10 ± 0.8; Osorio-Ocampo et al., 2019; Schmitt et al., 2006) and the Tres Vírgenes volcanic complex (TVVC; Avellán et al., 2018; 2019). This complex is formed by a N-S alignment fromed by La Virgen (LVV; 112 ± 21 ka; Avellán et al., 2018), El Azufre (EAV; 146 ± 22 ka; Avellán et al., 2018) and El Viejo volcanoes (EVV; 245 ± 39 ka; Avellán et al., 2018). These Quaternary

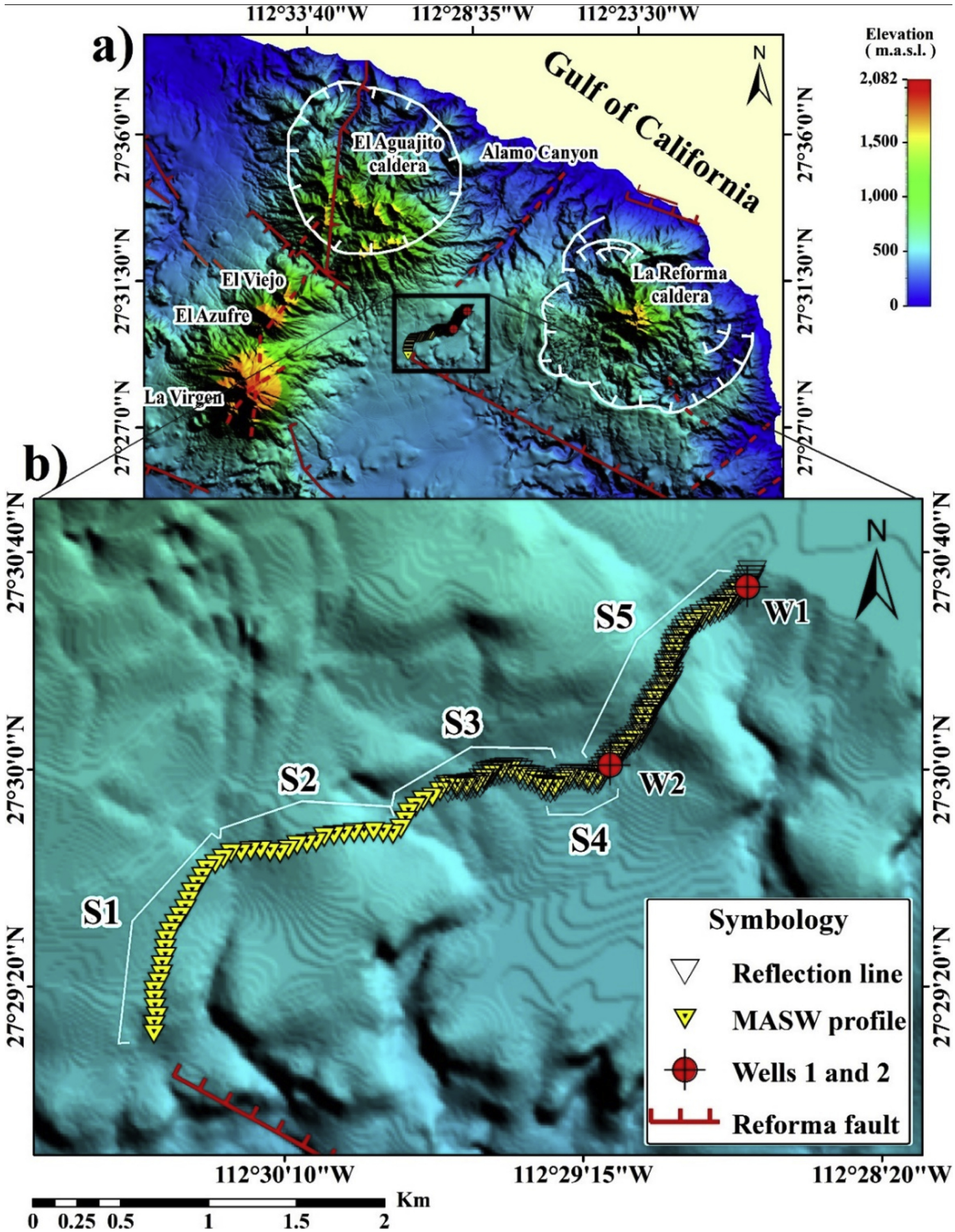

Fig. 2. a) Location of the study area (black rectangle) located at a strategic location between the Quaternary volcanoes in the area. b) Zoom in of the study area showing the MASW profile (yellow triangles), seismic reflection profile (hollow triangles) and wells 1 and 2 (W1 and W2, respectively, in red circles). S1 to S5 are the segments in which the MASW seismic line was divided. Faults and calderas boundaries were taken from Avellán et al. (2018).

volcanoes are situated on a granodioritic basement of Cretaceous age (99.1 ± 0.8; Avellán et al., 2018), overlayed by a volcano-sedimentary sequence known as the Comondú group, and shallow marine deposits of the Santa Rosalía Basin (Wilson and Rocha, 1955).

LRC is the result of Quaternary volcanism ocurred between 1.4 to 1.2 Ma that formed a 10–12 km wide nested caldera with a central resurgent dome (Garduño-Monroy et al., 1993; Schmitt et al., 2006; García Sánchez et al., 2019). The LRC is a very complex structure formed by three nested calderas and associated ignimbrites with lava flows and domes located near the margins and within the caldera

(García-Sánchez et al., 2019). On the other hand, we can distinguish two sequences, the granodoritic basement inside this caldera (Shmidt, 1975) and sedimentary rocks as suggested and better displayed by García-Sánchez et al. (2019). Also, several studies have reported the presence of surface spring waters in the LRC and in its limit with El Alamo canyon (located at approximately 2 km from the shallow wells drilled for this work) (e.g., Portugal et al., 2000; Prol-Ledesma et al., 2016). From the chemical analysis of waters, Portugal et al. (2000) propose the possible presence of a shallow magmatic chamber that underlies caldera and intrusive bodies below it. The LRC is situated east of the Tres Virgenes Volcanic Complex and the Las Tres Vírgenes geothermal field (LTVGF), which is one of the four geothermal fields in Mexico operated by Comisión Federal de Electricidad (CFE-Generación VI) with a capacity production of 10 MW (Gutiérrez-Negrin, 2019; Romo-Jones et al., 2018).

3. Materials and method

3.1. Materials

An acquisition of MASW data and multichannel seismic reflection profiling was performed in May 2017, at a strategic location near limits between LRC and LTVGF (we cannot assure that is also at the limits with the EAC; Fig. 2a). In this place the possible process of thermal recovery under the caldera and the effect of the thermal anomalies from geothermal field itself, could envisage with a possible geothermal potential, principally for direct uses. The equipment used included an impulsive seismic source *GISCO ESS500* of accelerated weight drop (a metallic plate of 220 kg falling at 5 m/s of velocity) and 24 vertical geophones with 4.5 Hz of natural frequency.

3.2. Data acquisition

3.2.1. MASW

In the field, MASW data were acquired using an aligned arrangement of 24 vertical geophones with a spacing (*gx*) of 10 m between them. The seismic data acquisition was carried out in twenty consecutive profiles of 230 m each along a total length of 4.8 km (Fig. 2b). The energy source was used every 10 m along the spread lines and 50 m away from both edges (moving-source configuration) obtaining 27 records per profile, with recording length (*t*) of 2000 ms at 0.125 ms sample interval (*dt*). This acquisition was made along an enabled path, according to the accessibility of the area; thus, the survey spread is not a straight line (Fig. 2b).

3.2.2. Seismic reflection

The seismic reflection survey was started northeastern from the MASW profile over the same path (Fig. 2b) with 2200 m of spread length, using a conventional linear arrangement with $gx = 5$ m and offset = 50 m, $t = 2000$ ms and $dt = 0.125$ ms.

3.2.3. Shallow wells

In the same area, two boreholes were drilled with the driller *Drilling 2800HS (HT)*, able to drill 70 m of depth, a property of CICESE-CeMIEGeo. Both wells are 55 m depth. Well 1 (W1) was performed NE the seismic surveys (corresponding to the nearest available zone to La Reforma caldera) at 502 masl, and geological cores were obtained at a maximum depth of 50 m. Well 2 (W2) is located 1400 m SW from W1 (Fig. 2b) at 524 masl, with the recovery of cores up to 55 m depth. The lithological profiles from W1 and W2 were carried out and interpreted with the support of CeMIE-Geo technical-staff.

3.3. Methods

3.3.1. MASW

The general method for construction of V_S profiles, once the seismic data has been acquired, consists of a) generation of dispersion image, b) extraction of dispersion curve(s) and, c) inversion of dispersion curve (s). Data processing was carried out in 1D and 2D using the *SeisImager* software package (Geometrics) with the procedure described by Hayashi (2003).

The 4.8 km line was divided into five segments, each with an arrangement as linear as possible, composed by six or less seismic profiles (Fig. 2b), and 2D models were generated in each of these segments. Also, 1D models were made at the position of each well to correlate with the corresponding lithological columns.

3.3.1.1. MASW 1D. Dispersion images were generated (Fig. 3a and b) from the closest seismic records to each well (W1 and W2). Entry parameters were minimum (*fmin*) and maximum (*fmax*) frequency values of 5 and 30 Hz respectively, according to the natural frequency of sensors and above which no information of interest is observed, respectively, as well as maximum phase velocity ($V^{fase}max$) of 2000 m/s according to the type of soil. To extract the corresponding dispersion curves, we selected the fundamental-mode phase velocity in the higher amplitude values (blue trends in Fig. 3a and b) within the range of frequencies specified. From this, dispersion curves were generated in diagrams of phase velocity - frequency (*c* - *f*) as shown in Fig. 3c and d. Finally, an iterative inversion of each dispersion curve was carried out by the nonlinear least squares method, with 15 iterations, starting from an initial model of 10 layers and $V^{fase}min$ *and* $V^{fase}max$ values according to the observed data. From this, a V_S *vs* Z model was obtained, at the center of each receiver spread (Xia et al., 1999).

3.3.1.2. MASW 2D. Fig. 2b shows the location of the five segments processed separately to generate 2D models. The procedure is the following. a) Selecting the set of seismic records corresponding to each segment, b) assigning shot points and receivers geometry. c) Common Mid-Point Cross-Correlation analysis described by Hayashi and Suzuki (2004). d) The MASW method is applied to the CMPCC gathers, to calculate phase velocities, using values of $f_{min} = 5$ Hz, $fmax = 30$ Hz and $V^{fase}max = 2000$ m/s; after this process, we obtained the corresponding set of dispersion curves (Fig. 4) instead of individual dispersion images. e) Basic filtering was applied individually to each dispersion curve to eliminate noise and higher modes; the information of interest was concentrated, mostly, within 5–25 Hz. f) A non-linear least squares method was applied to the dispersion curves to reconstruct the 2D S-wave velocity profile; an initial model is generated with ten layers, and inversion with 15 iterations. g) Finally, we obtained one 2D S-wave velocity model per segment.

3.4. Seismic reflection

Seismic reflection data were processed using *Landmark's ProMax®* software, and following a conventional processing sequence (Yilmaz, 2001) that included the following stages: a) Pre-stack: trace editing, geometry, static correction, deconvolution, filter application (top-mute, band-pass, and F-K); b) Stack: ordering by CDP, velocity analysis and Normal Move-Out (NMO) correction; c) Post-stack: spherical divergence correction, migration in time and migration in depth. Geological interpretation included a study of the main seismic-stratigraphic and structural characteristics observed in the seismic reflection section.

4. Results

4.1. MASW

4.1.1. 1D Models

Resulting 1D MASW models are presented in Fig. 5a and b for the two wells. Both models show a gradual variation of seismic velocity with depth. This variation can be grouped into three zones, where the central zone (CZ) has lower V_S values than the upper part (UZ), and this

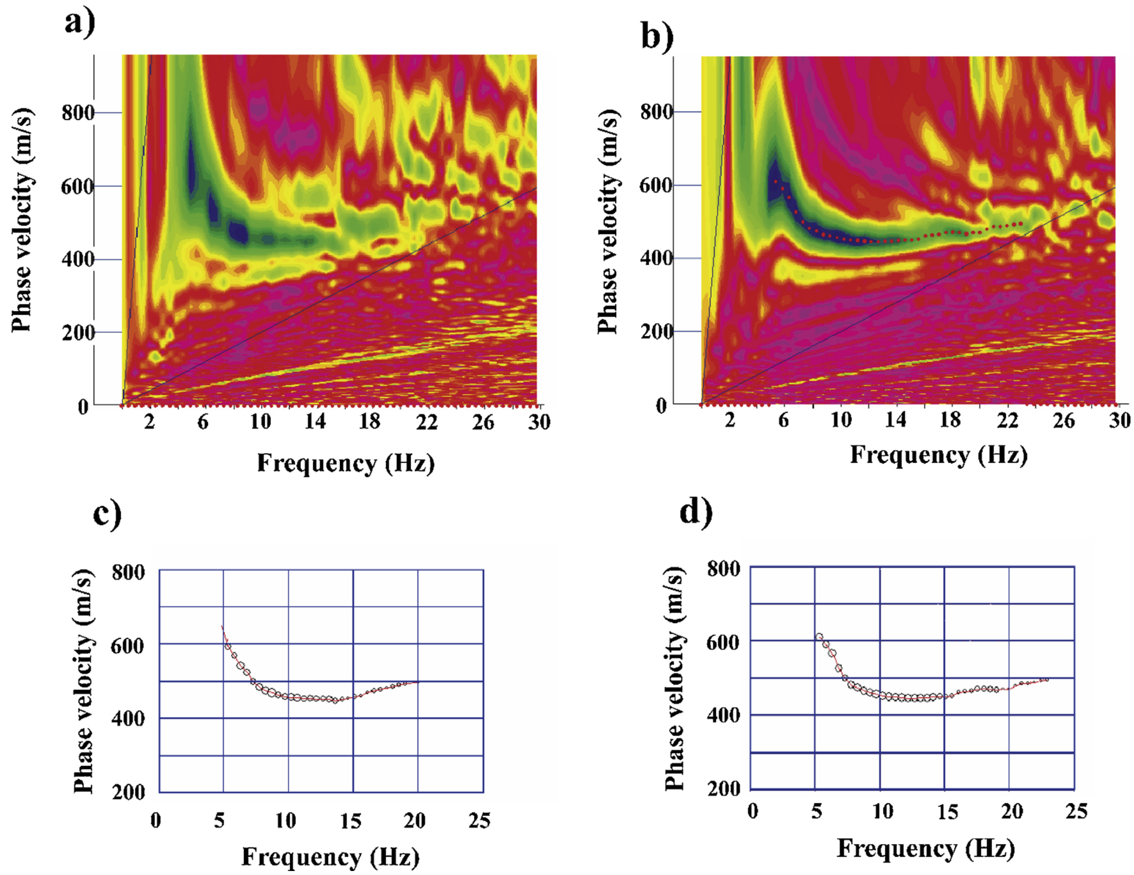

Fig. 3. a, b) Dispersion images resulting from time to frequency domain transformation of W1 and W2 seismic records, respectively. c, d) Dispersion curves extracted from selection of the Rayleigh waves fundamental mode (maximum amplitude in blue) within the spectral images of W1 and W2, respectively.

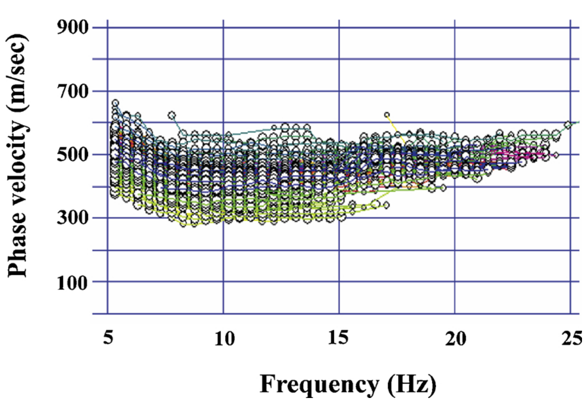

Fig. 4. Set of dispersion curves obtained from 2D processing of segment 5 (seismic records contained between the two wells).

in turn smaller than the deepest one (LZ). The resulting model of W1 suggests an average value of V_S in UZ ≈ 547 m/s, CZ ≈ 474 m/s and LZ ≈ 666 m/s; and the W2 model in UZ ≈ 561 m/s, CZ ≈ 458 m/s y LZ ≈ 655 m/s. The RMS values of both profiles were less than 3%. Each model represents the average S-wave velocity variation within subsurface structures beneath the center of the corresponding geophone spread (Xia et al., 2000).

Borehole lithological data, presented in Fig. 6b, was correlated with the corresponding S-wave velocity model (Fig. 7a and b). This comparison showed reasonable matching of the velocities zones from MASW models and lithological limits from each borehole column; therefore, it was possible to associate low-velocity zones (CZ) from both profiles with the volcanic ash layer.

4.1.2. 2D Models

2D models of V_S resulting from the five segments (Fig. 2b) are shown in Fig. 8a-e. The five 2D MASW profiles reach an imaged depth range from 1 to 55 m. Low-velocity zones (green and blue) were identified in every section, with V_S gradual variation in depth, and lateral distribution semi-parallel to the surface. Also, velocity discontinuities and anomalous V_S areas were observed at depths higher than 30 m that may be related to geological structures such as faults. The region of highest V_S values was found within models S3 and S4, with values from 800 to 1200 m/s.

The 2D model of S5 (Fig. 8e) contains the information between the two wells, showing a semi-continuos V_S lateral distribution, where we identified a low-velocity zone within the depth range from 10 to 40 m, approximately. To complement this information, we correlated this model with the corresponding lithological column of W1 and W2 (Fig. 9). This comparison allowed to relate favorably every type of rock limit from borehole data with main changes of V_S in depth. The low-velocity zone, delimited by H1 and H2, is associated with volcanic ash units, and beneath this, sequences of basalts and rhyolites. Besides, with seismic velocity distribution, it was possible to corroborate the lithological disposition of subsoil within the two wells, as well as between them, and the effectiveness of this method applied in a volcanic region near geothermal systems.

A complete V_S image was generated along the 4.8 km. This model, presented in Fig. 10, shows a semi-uniform distribution of V_S in the first 30 m depth, although the areas of low seismic velocity are pointed out (yellow ellipses). Up to this depth level, the most prominent V_S lateral contrasts are shown and interpreted as possible superficial faults (black dashed lines). Red dotted line delimits maximum V_S values within the whole model, related to a medium of higher density. Also, wells W1 and W2 are positioned, volcanic ash horizon is delimited in white dotted

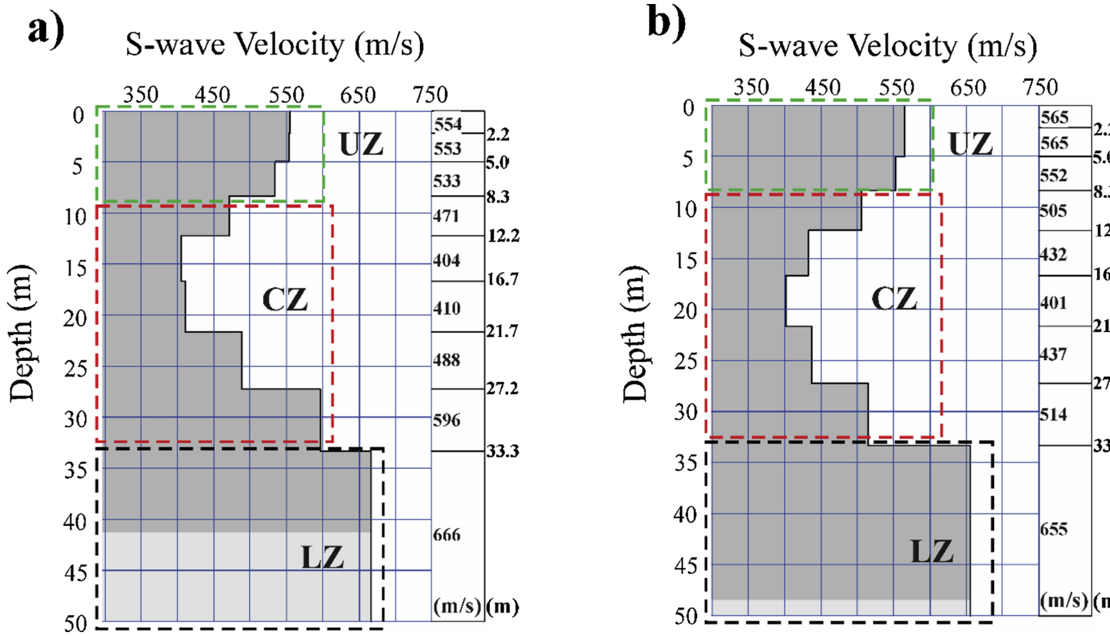

Fig. 5. 1D models of V_S (shear- or S-wave velocity) corresponding to Wells 1 and 2 (a and b, respectively) generated with the MASW method. The end of dark gray areas corresponds to the effective depth of investigation. Every step corresponds to one of the ten layers from initial model. The dotted lines separate the three distinct velocity zones, according to its distribution: UZ = upper zone, CZ = central zone, LZ = lower zone.

lines, and the red box (Fig. 10c) encloses the MASW portion that matches the seismic reflection profile. According to the V_S distribution (Fig. 10), we inferred that the lithology from W1 y W2 extends laterally along the study area.

4.2. Seismic reflection model

The resulting seismic reflection section is presented in Fig. 11a, which matches a portion of the MASW model (Fig. 2b, Fig. 10b, c), and intersects the two wells. This section highlights a remarkable contrast of high and low seismic amplitudes, delimited by horizon R1 in green (Fig. 11b). Above R1, lies a zone with V_P values of 2000–3000 m/s, possibly related to sequences of basalts and rhyolites (according to borehole lithology). Below R1, there is a region of low amplitude that migth be associated with ignimbrites, according to lithology from LV-2 (CFE internal report, 1993) and to the stratigraphics sequence reported (Macías-Vázquez and Jimenez-Salgado, 2013; Avellán et al., 2018; García-Sánchez et al., 2019). Even though the seismic profiles are located in the boundary between Aguajito and Reforma calderas, the seismic method does not allow us to identify the type of rock in depth, or distinguish whether the ignimbrites belong to Aguajito or Reforma caldera. Also, wells W1 and W2 (55 m in depth) did not cut any sample of ignimbrite and did not reached the zone where we interpreted them (200–400 m) in depth. Thus, to determine the lithology of the sequences seen in the seismic section we would need geological cores from depths of 200–400 m.

5. Discussion

Vertical resolution reached in this seismic profile was approximately 500 m, and "whitening" of the signal is observed, for the most part, from 200 and 300 m depth. Chaotic reflectors pattern may be due to the dispersive nature of volcanic environments. However, it was possible to identify several faults of different length and dip (yellow line), whose abundance evidences intense fracturing of rocks beneath the study area. This finding would explain the high loss of circulation presented during the drilling of the wells.

The MASW model allowed us to characterize the subsurface structures from the distribution of V_S in the first 60 m depth, constrained with lithology from W1 and W2. Reflection profile does not resolve the small-scale structures (first 40 m depth) imaged by MASW models; therefore, this section (Fig. 11b) was complemented by overlaying the corresponding MASW profile (Fig. 10c), as shown in Fig. 12c. In this way, an entire seismic image was obtained, consisting of seismic structures from 1 to 60 m (MASW) at the shallowest portion, and from 60 to 500 m (reflection) at the deepest part.

From this comparison (Fig. 12c), it was found that the variation of both V_S from MASW model and amplitudes from the reflection section is consistent. Highest velocity values in the MASW profile are delimited by the dotted red line and decreases laterally rightward. Likewise, in the reflection section, the highest seismic amplitudes are below 2400 to 3300 m distance, and the very low amplitude zones agree to underlie the weaker V_S portion.

The amplitude of seismic reflectors is related to the rocks velocity and density. Kell (2014) and Sahakian et al. (2016) have reported seismic images with similar features to the area below R1, where the amplitude of seismic reflectors decreases drastically from one area to another, occurring "obscuring" of stratigraphy. The seismic signal interruption and the creation of vertical acoustic striping, are related to fluid accumulation, indirect evidence of lateral fault deformation, potential permeability pathways for fluids migration, presence of gas or thermal alteration fronts, mainly in sites located near geothermal systems (Kell, 2014; Sahakian et al., 2016).

Although most of them were performed in sedimentary environments, the characteristics identified by these authors are comparable with those observed in the present study, which reports favorable results of two seismic surveys conducted in a volcanic environment site close to areas with geothermal potential

Further comparison between the results of the two seismic methods showed a relationship between the structures observed in the MASW profile (black lines) with some faults interpreted in the reflection section (yellow).

The map showed in Fig. 12b integrates the surface projection of these correlated faults (orange lines), and low-velocity seismic regions (pink ellipses) cut at 200 m in depth from the Fig. 11b, which are interpreted as possible hydrothermal alteration fronts.

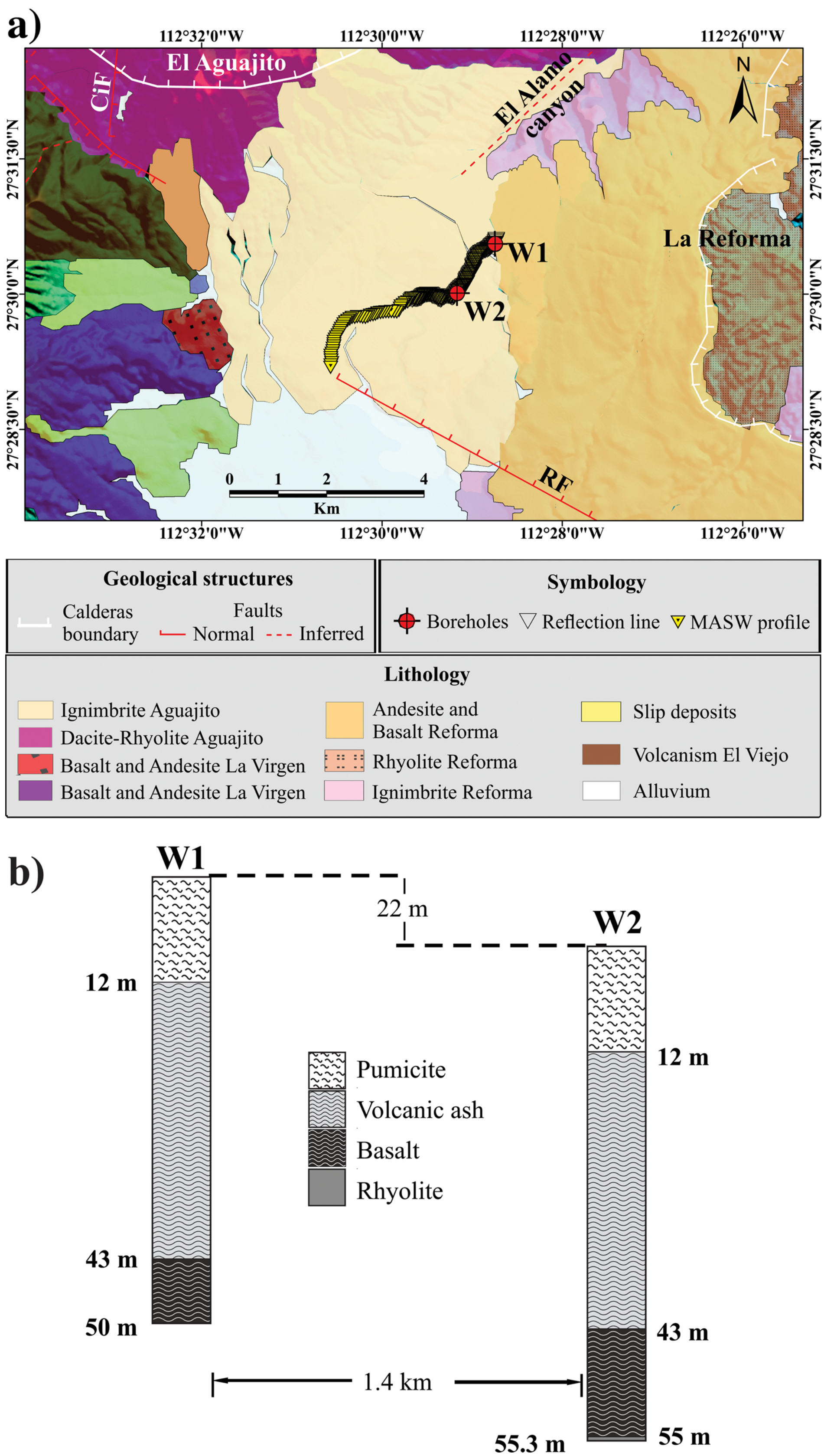

Fig. 6. a) Geological map of the study area (taken and modified from Antayhua-Vera, 2017) with the proyection of both wells (W1 and W2; red circles) and the seismic lines (yellow and hollow triangles). b) Lithological columns generated from the geological data of volcanic rocks recovered from W1 and W2, in the study area.

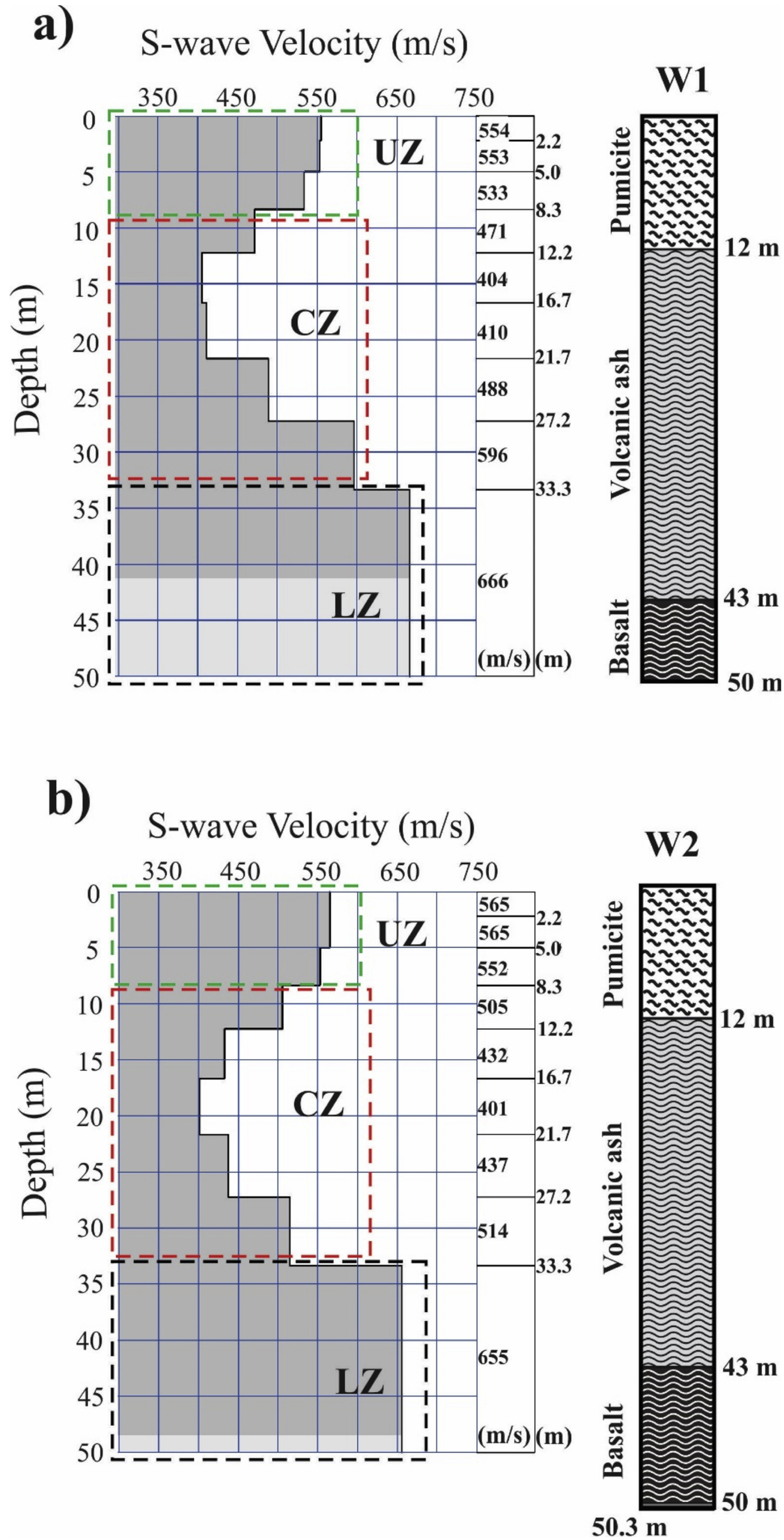

Fig. 7. 1D models of V_S and its correlation with lithological columns from (a) Well 1 and (b) Well 2. Zones: Upper (UZ), Central (CZ), and Lower (LZ), related to pumice, volcanic ash, and basaltic layers, respectively.

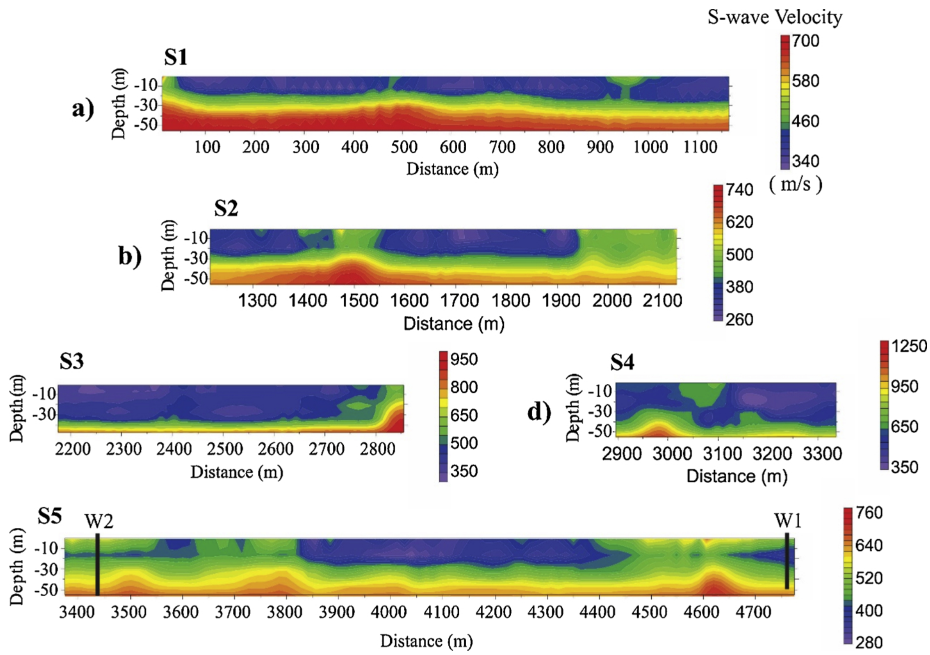

Fig. 8. 2D models of V_S corresponding to segments a) S1, with 1190 m in length; b) S2, of 950 m; c) S3, of 690 m long; d) S4, the smallest line of 460 m; e) S5, whose 1400 m in length corresponds to the information contained between Wells 1 and 2, which are represented with black vertical lines. Color scales represent minimum and maximum V_S values from each section. Blue colors are low-velocity values, and red ones are the highest V_S zones.

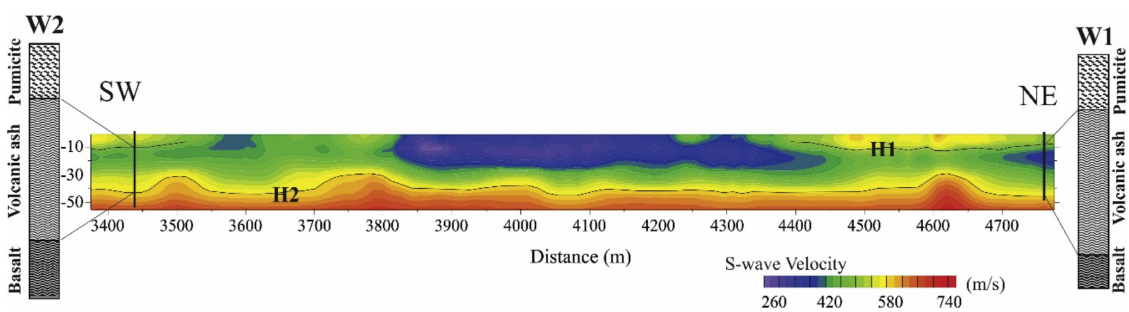

Fig. 9. 2D model of V_S from segment 5 and its correlation with the lithological columns of wells W1 and W2. Horizons H1 and H2 delimit the low-velocity zone that matches the volcanic ash layer.

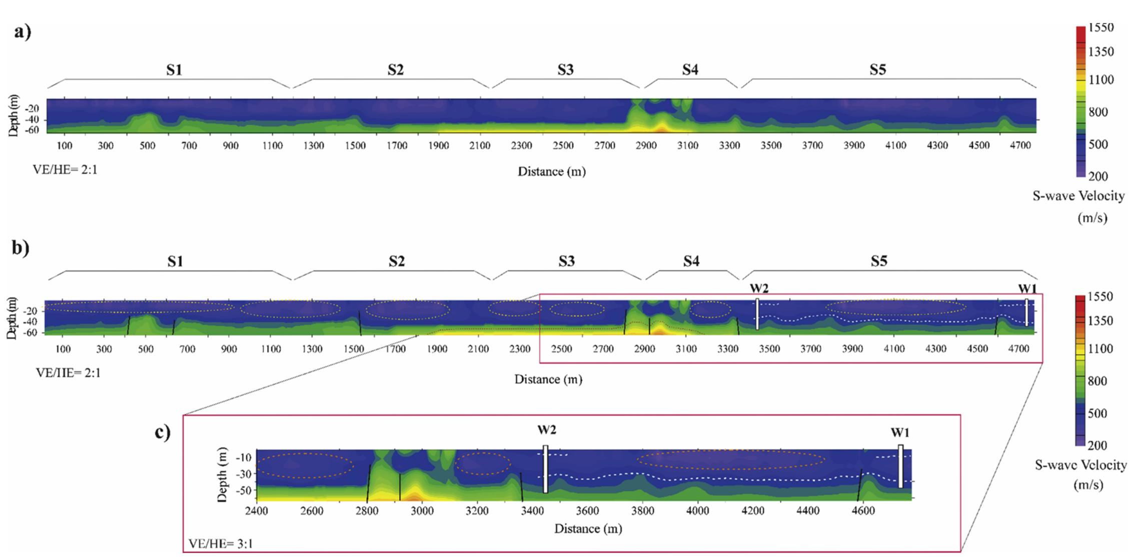

Fig. 10. 2D model of V_S from the 4.8 km long seismic line. a) Original. 'S1-S5′ indicates the location of segments 1 to 5, respectively. b) Interpretation showing: very low-velocity zones (yellow ellipses); potential faults (black lines) interpreted from the most prominent lateral contrasts of V_S; the region with maximum values of V_S (in red dotted line), W1 and W2 within the seismic profile; and the layer of volcanic ash (white dotted lines). The red box contains c) zoom to the portion of this model that matches the seismic reflection profile. Fig. 12 shows a combination of both sections.

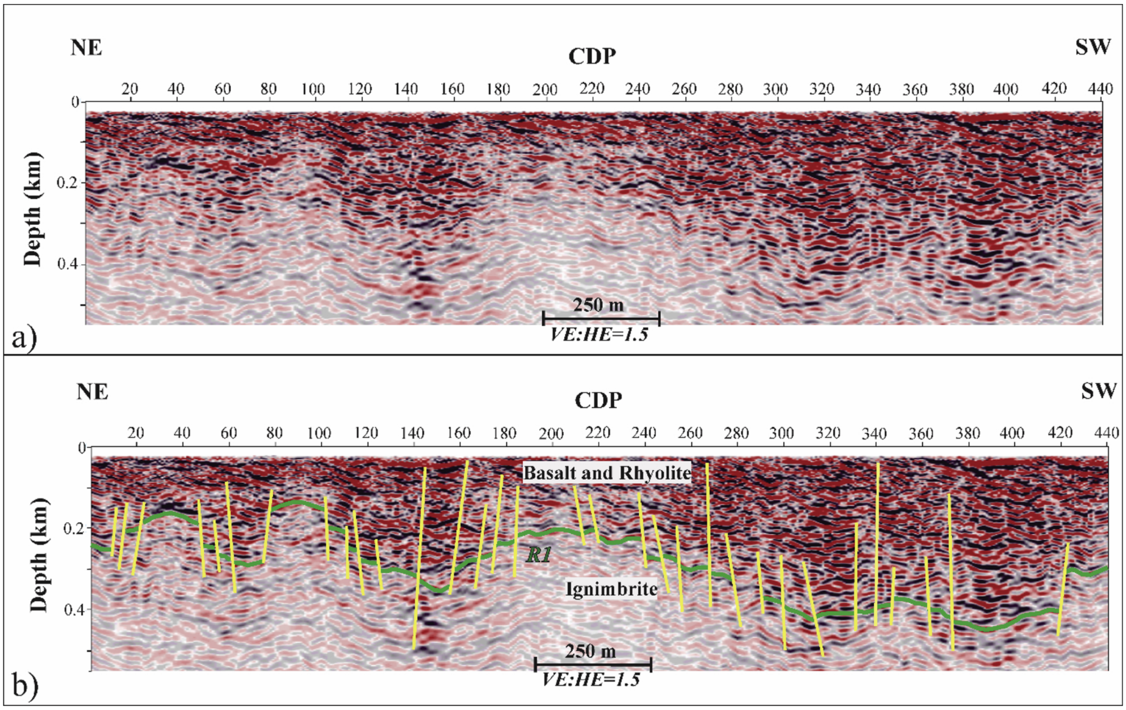

Fig. 11. Resulting 2D seismic reflection section. a) Original. b) Interpreted. Horizon R1 (green line) points the limit between high and low seismic amplitude areas (upper and lower, respectively). Yellow lines represent interpreted geological faults. The geological units associated with each region are indicated.

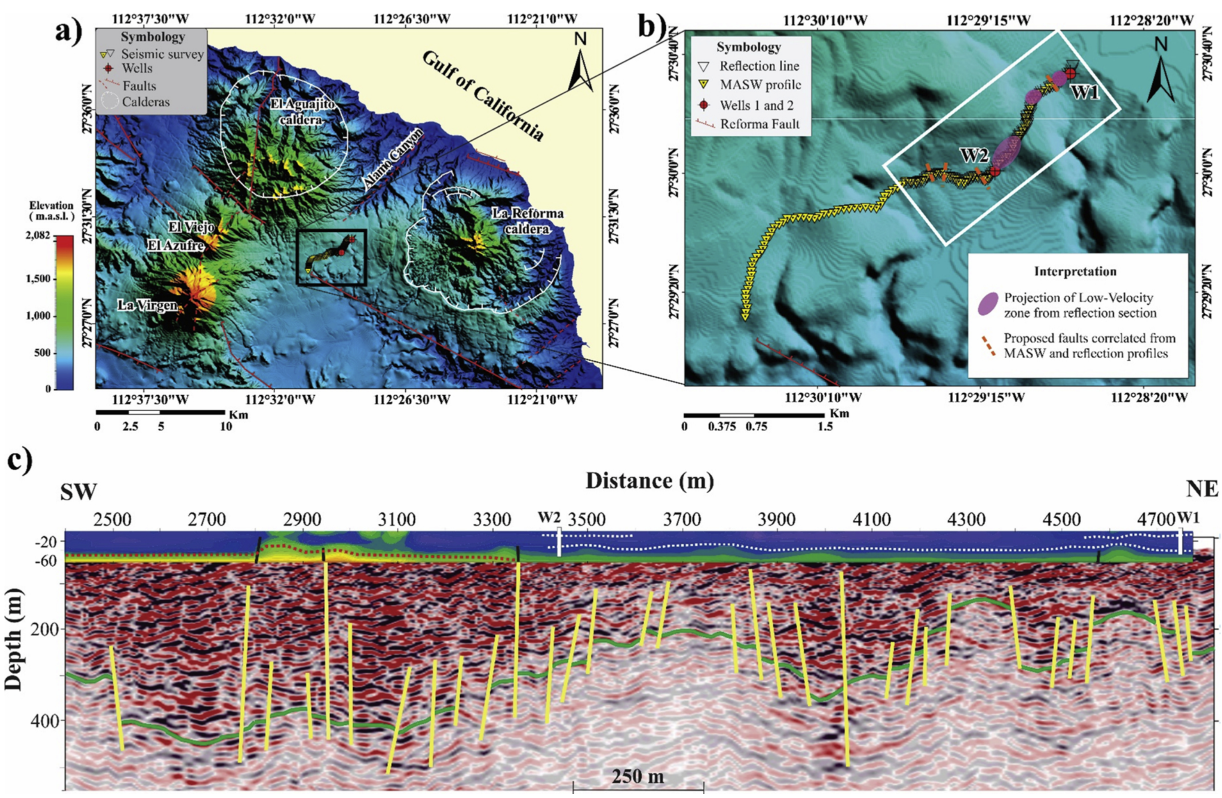

Fig. 12. MASW and seismic reflection profiles. a) Location map of seismic profiles and the two wells. b) Zoom to the study area. The white box contains the seismic lines displayed in c) and the location at the surface of the low-velocity regions (cut at 200 m depth) (green ellipses), as well as the faults correlated on both profiles (MASW and reflection) (red lines). c) Overlay of the 2D MASW model (0–60 m) and the seismic reflection section (60–550 m). W1 and W2, wells. The zone with maximum V_S in the MASW model it is delimited with the dotted red line, and the volcanic ash layer in dotted white lines. Faults interpreted in the MASW model (black lines) consistent with those (in yellow) of the reflection section. Green horizon: limit between high (upper) and low (lower) seismic amplitude areas.

Seismic results of this work are consistent with the models and maps of electrical resistivity reported by Antayhua-Vera (2017), where small conductive anomalies, found within our study zone, agree in 500 m of depth with the location of our low velocity zones (pink ellipses).

Some authors (Manzella, 1973; Garduño-Monrroy et al., 1993; López-Hernández et al., 1995; Romo-Jones et al., 2000; Flores, 2003) relate the anomalies of high electrical conductivity occurring in regions of fault junction to intense fracturing and hydrothermal fluids in the subsurface. From seismic results of this work, we identify areas of abundant fractures in depth. Furthermore, seismic regions of low velocity, along with the zones of low electrical resistivity from Antayhua-Vera (2017) allow suggesting possible hydrothermal alteration fronts above 300 m depth within the study area. This proposal is supported by the proximity of the study area to the geothermal system in operation (LTVGF), thermal springs (Prol-Ledesma et al., 2016), inferred superficial faults around the study area (Garduño-Monroy et al., 1993; Romo-Jones et al., 2000; Macías Vázquez and Jiménez Salgado, 2013), a magma chamber under Tres Virgenes volcanic complex better described by Avellán et al. (2018) and a possible magma chamber below the La Reforma caldera proposed by Portugal et al. (2000).

The seismic results can be related to lithological sequences reported by several authors around the study area (CFE internal report, 1993; Macías Vázquez and Jiménez Salgado, 2013; Avellán et al., 2018; 2019; García-Sanchez et al., 2019); however, to define the type of rocks, the disposition of the volcanic sequences, and the precisely location where the possible thermal fluids are hosted, it is necessary to prospect this specific zone with more geophysical methods, that complement the results of the present work, but also deeper exploratory boreholes with recovery of core samples.

These results constitute a useful preliminary knowledge of the study area and open up the need and possibility of carrying out temperature measurements in the boreholes (W1 and W2), which are necessary to estimate thermal gradient and heat flow, and hence, its thermal behavior and its relationship with seismic structures of possible geothermal interest, mainly for direct utilization.

6. Conclusions

The final results of this work represent the first seismic reports within the La Reforma caldera (close to the boundary with the Tres Vírgenes geothermal field); as well as the first lithological information (first 55 m depth) of the area. The seismic source of weight drop, achieved a maximum depth range of 60 m imaged in the 2D models of MASW, higher than that usually obtained with a sled hammer. The correlation between 1D and 2D models of V_S with the lithological columns from W1 and W2 yield a good relationship between the limits of each type of rock and vertical changes of seismic velocity. From this, a wide low-velocity zone was associated with the volcanic ash layer. The semi-continuous distribution of seismic velocities along the MASW profile suggested that lithological arrangement obtained from W1 and W2 is the same in the first 50 m depth throughout the study area. Thereby, low-velocity seismic structures may be found anywhere. For this reason, it is not advisable to use the seismic refraction method to characterize the shallow subsurface of this region. Then, we recommend using the MASW method, because of its effectiveness, even in volcanic environment areas. The comparison between the MASW model and the seismic reflection section showed that the variation of S-wave velocity (MASW) and amplitudes (reflection section) was consistent. The lowest V_S values (MASW) confirmed the presence of deeper low-velocity zones (reflection). Seismic results of this work showed intense fracturing in the subsurface of this area, as well as deep low-velocity regions, consistent with low electrical resistivity anomalies. These facts and the proximity with the geothermal field (LTVGF) allowed suggesting possible hydrothermal alteration below 300 m in depth. Future works should involve more geophysical researches in this area that complement the present work and that allow identifying with greater precision the location of hydrothermal alteration at depth and estimate the geothermal energy available. At present, we are developing thermal analysis within the two boreholes to estimate shallow thermal gradient and heat flow, that let us know the thermal behavior in the subsurface of the area of interest.

Declaration of Competing Interest

There is no petential conflicto of interest.

Acknowledgments

The first author (S-LEB) thanks CONACYT for funded the master's fellowship 769580 and also to Division of Earth Sciences/CICESE for funding the writing of this manuscript. The authors we thanks funding by the following Projects: Catedras-CONACYT 2074 (G-AE); 644-294 “Campaña Intensiva de Exploración Geotérmica de las Cuencas Wagner, Consag, Delfín, Guaymas and Alarcón del Sistema de Rifts del Golfo de California” (P03 from Centro Mexicano de Innovación en Energía Geotérmica -CeMIEGeo-), and PN2016-2188 “Estimación y evaluación del potencial geotérmico de sistemas de baja y mediana entalpía para usos directos y generación de energía eléctrica con tecnología de ciclo binario: El caso de las calderas La Reforma y El Aguajito del complejo volcánico Las Tres Vírgenes, Baja California Sur”, from the national program Proyectos de Desarrollo Científico Para Atender Problemas Nacionales (CONACYT). An especially grateful to Jaime Calderón-González and Enrique Cruz Castillo-Guerrero technical staff of Department of Applied Geophysics/CICESE for your help to seismic data acquisition. Porfirio Aviléz Serrano and Hilario Zúñiga Ruíz specialized staff of CeMIE-Geo for his support in the drilling of wells in the field; and Gilberto Zambrano Romero and the field staff of the UMA (Unidad de Manejo y Aprovechamiento Sustentable del Borrego Cimarrón) for their help to carry out this study in La Reforma caldera. Also, we are grateful to Ejido Bonfil for the permission granted to access the Las Tres Vírgenes volcanic complex, BCS. Constructive comments and suggestions by one anonymous reviewer improved this manuscript.

References

Almalki, H., Munir, K., 2013. Efficiency of MASW in detecting near-surface cavities. ASEG Ext. Abstr. 2013, 1–4. https://doi.org/10.1071/aseg2013ab043.

Antayhua-Vera, Y.T., 2017. Caracterización sismológica, aeromagnética y magnetotelúrica del Campo Volcánico y Geotérmico de Las Tres Vírgenes (B.C.S.). Universidad Nacional Autónoma de México, México.

Avellán, D.R., Macías, J.L., Arce, J.L., Jiménez-Haro, A., Saucedo-Girón, R., Garduño-Monroy, V.H., Sosa-Ceballos, G., Bernal, J.P., López-Loera, H., Cisneros, G., Layer, P.W., García-Sánchez, L., Reyes-Agustín, G., Rocha, V.S., Rangel, E., 2018. Eruptive chronology and tectonic context of the late Pleistocene Tres Vírgenes volcanic complex, Baja California Sur (México). J. Volcanol. Geotherm. Res. 360, 100–125. https://doi.org/10.1016/j.jvolgeores.2018.06.012.

Brogi, A., Lazzarotto, A., Liotta, D., Ranalli, G., 2003. Extensional shear zones as imaged by reflection seismic lines: The Lardello geothermal field (central Italy). Tectonophysics 363, 127–139. https://doi.org/10.1016/S0040-1951(02)00668-6.

Avellán, D.R., Macías, J.L., Arce, J.L., Saucedo-Girón, R., Garduño-Monroy, V.H., Jiménez-Haro, A., Sosa-Ceballos, G., Cisneros, G., Bernal, J.P., Layer, P.W., García-Sánchez, L., Reyes-Agustín, G., Rangel, E., Navarrete, J.A., López-Loera, H., 2019. Geology of the late Pleistocene Tres Várgenes Volcanic Complex, Baja California Sur (Míxico). J. Maps 15 (2), 227–237. https://doi.org/10.1080/17445647.2019.1576552.

Bruno, P.P.G., Castiello, A., 2009. High-resolution onshore seismic imaging of complex volcanic structures: An example from Vulcano Island. Italy. J. Geophys. Res. Solid Earth 114, 1–12. https://doi.org/10.1029/2008JB005998.

Bruno, P.P.G., Rapolla, A., Di Fiore, V., 2003. Structural setting of the Bay of Naples (Italy) seismic reflection data: Implications for Campanian volcanism. Tectonophysics 372, 193–213. https://doi.org/10.1016/S0040-1951(03)00327-5.

Cameli, G.M., Ceccarelli, A., Dini, I., Mazzotti, A., 2000. Contribution of the seismic reflection method to the location of deep fractured levels in the geothermal fields of Southern Tuscany (Central Italy). In: Proceedings World Geothermal Congress 2000. Kyushu-Tohoku, Japón. pp. 1025–1029.

Flores, C., 2003. Mapping Upflow Zones with the Anomalous Geometry of a Shallow Conductor at the Las Tres Virgenes Geothermal Field, Mkxico. Geotherm. Resour. Counc. Trans. 27, 219–222.

Gallegos-Castillo, C.A., 2019. Identificación y ubicación de intrusivos ígneos someros mediante sísmica de reflexión 2D en el rift norte de la cuenca de Guaymas, Golfo de

California. Centro de Investigación Científica y de Educación Superior de Ensenada, Baja California.
García Sánchez, L., Macías, J.L., Sulpizio, R., Osorio-Ocampo, L.S., Pellicioli, C., Pola, A., Avellan, D.R., Cisneros, G., García, F., Ocampo-Díaz, Y.Z.E., Lira-Beltran, R.M., Saucedo, R., Sánchez-Núñez, J.M., Arce, J.L., Corona-Chávez, P., Reyes-Agustin, G., Cardona, M., Layer, P.W., Benowitz, J., Solari, L., Groppelli, G., 2019. Geology of La Reforma caldera complex, Baja California. Mexico. J. Maps 15, 487–498. https://doi.org/10.1080/17445647.2019.1612287.
Garduño-Monroy, V.H., Vargas-Ledezma, H., Campos-Enriquez, J.O., 1993. Preliminary geologic studies of Sierra El Aguajito (Baja California, Mexico): a resurgent-type caldera. J. Volcanol. Geotherm. Res. 59, 47–58. https://doi.org/10.1016/0377-0273(93)90077-5.
Gutiérrez-Negrin, L.C.A., 2019. Current status of geothermal-electric production in Mexico. IOP Conf. Ser. Earth Environ. Sci. 249. https://doi.org/10.1088/1755-1315/249/1/012017.
Hayashi, K., 2003. Data Acquisition and Analysis of Active and Passive Surface Wave Methods, in: Active and Passive Surface Waves. SAGEEP 1–106.
Hayashi, K., Suzuki, H., 2004. CMP cross-correlation analysis of multi-channel surface-wave data. Explor. Geophys. 35, 7–13. https://doi.org/10.1071/EG04007.
INEGI, 2019. Instituto Nacional de Estadística y Geografía, México. https://www.inegi.org.mx/temas/topografia/.
Ismail, A., Brett Denny, F., Metwaly, M., 2014. Comparing continuous profiles from MASW and shear-wave reflection seismic methods. J. Appl. Geophys. 105, 67–77. https://doi.org/10.1016/j.jappgeo.2014.03.007.
Kearey, P., Brooks, M., Hill, I., 2002. An Introduction to Geophysical Exploration, 3rd ed. Blackwell Science Ltd, Estados Unidos.
Kell, A.M., 2014. The Application of Active–source Seismic Imaging Techniques to Transtensional Problems the Walker Lane and Salton Trough. University of Nevada, Reno.
Kluesner, J.W., 2011. Marine Geophysical Study of Cyclic Sedimentation and Shallow Sil Intrusion in the Floor of the Gulf of California. University of California, San Diego. https://doi.org/10.4018/978-1-5225-7659-4.ch043.
Lamarche, G., 1992. Seismic Reflection Survey in the Geothermal Field of the Rotorua Caldera, New Zeland. Geothermics 21, 109–119.
Liberty, L.M., Schmitt, D.R., Shervais, J.W., 2015. Seismic imaging through the volcanic rocks of the Snake River Plain: insights from Project Hotspot. Geophys. Prospect. 63, 919–936. https://doi.org/10.1111/1365-2478.12277.
Lin, C.P., Chang, C.C., Chang, T.S., 2004. The use of MASW method in the assessment of soil liquefaction potential. Soil Dyn. Earthq. Eng. 24, 689–698. https://doi.org/10.1016/j.soildyn.2004.06.012.
Liotta, D., Ranalli, G., 1999. Correlation between seismic reflectivity and rheology in extended lithosphere: southern Tuscany, inner Northern Apennines, Italy. Tectonophysics 315, 109–122. https://doi.org/10.1016/S0040-1951(99)00292-9.
Lizarralde, D., Soule, S.A., Seewald, J.S., Proskurowski, G., 2011. Carbon release by off-axis magmatism in a young sedimented spreading centre. Nat. Geosci. 4, 50–54. https://doi.org/10.1038/ngeo1006.
López-Hernández, A., García-Estrada, G.H., Arellano-Guadarrama, F.J., 1995. Geothermal Exploration at Las Tres Virgenes, B.C.S., Mexico, in: World Geothermal Congress. Michoacán, pp. 707–712.
Macías Vázquez, J.L., Jiménez Salgado, E., 2013. Estudio de Estratigrafía y Geología del Complejo Volcánico Tres Vírgenes. B.C.S. Geotermia 26, 14–23.
Manzella, A., 1973. Geophysical Methodologies in Geothermal Exploration. Pisa, Italia.Geophysical Methodologies in Geothermal Exploration. Pisa, Italia.
MØller Hansen, D., 2006. The morphology of intrusion-related vent structures and their implications for constraining the timing of intrusive events along the NE Atlantic margin. J. Geol. Soc. 163, 789–800. https://doi.org/10.1144/0016-76492004-167.
Orfanos, C., Apostolopoulos, G., 2012. Analysis of different geophysical methods in the detection of an underground opening at a controlled test site. J. Balk. Geophys. Soc. 15, 7–18.
Osorio-Ocampo, L.S., García-Sánchez, L., Lira-Beltran, R.M., Macías, J.L., Pola, A., Avellán, D.R., Ocampo-Díaz, Y.Z.E., Groppelli, G., Sulpizio, R., García-Tenorio, F., González-Barba, G., Sosa-Ceballos, G., 2019. Volcanic and marine stratigraphy along the El Álamo Canyon, Santa Rosalía Basin, Baja California Sur. In: Pearthree, P.A. (Ed.), Geologic Excursions in Southwestern North America. Geological Society of America.
Park, C.B., 2001. Seismic Characterization of Geotechnical Sites By Multichannel Analysis of Surface Waves (MASW) Method.Seismic Characterization of Geotechnical Sites By Multichannel Analysis of Surface Waves (MASW) Method.
Park, C.B., Miller, R.D., Xia, J., 1999. Multichannel analysis of surface waves. Geophysics 64, 800–808.
Park, C.B., Miller, R.D., Xia, J., 1998. Ground roll as a tool to image near-surface anomaly. SEG Tech. Progr. Expand. Abstr. 874–877. https://doi.org/10.1190/1.1820627.
Planke, S., Eldholm, O., 1999. Seismic characteristics of basaltic extrusive and intrusive rocks. Proc. Int. Conf. Lead. Edge Manuf. 21st Century Lem21.
Planke, S., Rasmussen, T., Rey, S.S., 2015. Seismic characterization and distribution of volcanic intrusions and hydrothermal vent complexes in the Vøring and Møre basins. Petroleum Geology Conferences Ltd (Ed.), Petroleum Geology: North-West Europe and Global Perspectives. The Geological Society, London, pp. 833–844.
Portugal, E., Birkle, P., Barragán, R.R.M., Arellano, G.V.M., Tello, E., Tello, M., 2000. Hydrochemical-isotopic and hydrogeological conceptual model of the Las Tres Vírgenes geothermal field, Baja California Sur, México. J. Volcanol. Geotherm. Res. 101, 223–244. https://doi.org/10.1016/S0377-0273(99)00195-X.
Prol-Ledesma, R.M., Arango-Galván, C., Torres-Vera, M.A., 2016. Rigorous Analysis of Available Data from Cerro Prieto and Las Tres Virgenes Geothermal Fields with Calculations for Expanded Electricity Generation. LREC Int. Conf. Lang. Resour. Eval. 25, 445–458. https://doi.org/10.1007/s11053-016-9295-2.
Romo-Jones, J.M., Gutiérrez-Negrín, L.C., Sánchez-Cornejo, C., González-Alcántar, N., García-Gutiérrez, A., 2018. 2017 Mexico country report. IEA Geotherm. 10.
Romo-Jones, J.M., Wong-Ortega, V., Flores-Luna, C., Vázquez-González, R., 2000. Conductividad eléctrica y atenuación de ondas de CODA en el Campo Geotérmico Las Tres Vírgenes en Baja California Sur, México. GEOS 20, 21–29.
Roy, N., Jakka, R.S., 2017. Near-field effects on site characterization using MASW technique. Soil Dyn. Earthq. Eng. 97, 289–303. https://doi.org/10.1016/j.soildyn.2017.02.011.
Sáez Blázquez, C., Farfán Martín, A., Carrasco García, P., González-Aguilera, D., 2018. Thermal conductivity characterization of three geological formations by the implementation of geophysical methods. Geothermics 72, 101–111. https://doi.org/10.1016/j.geothermics.2017.11.003.
Sahakian, V., Kell, A., Harding, A., Driscoll, N., Kent, G., 2016. Geophysical evidence for a San Andreas subparallel transtensional fault along the northeastern shore of the Salton Sea. Bull. Seismol. Soc. Am. 106, 1963–1978. https://doi.org/10.1785/0120150350.
Schmitt, A.K., Stockli, D.F., Hausback, B.P., 2006. Eruption and magma crystallization ages of Las Tres Vírgenes (Baja California) constrained by combined 230Th/238U and (U-Th)/He dating of zircon. J. Volcanol. Geotherm. Res. 158, 281–295. https://doi.org/10.1016/j.jvolgeores.2006.07.005.
Sena-Lozoya, E.B., 2019. Exploración sísmica y térmica somera y su correlación con columnas litológicas de pozos en la caldera La Reforma, Baja California Sur, México. Centro de Investigación Científica y de Educación Superior de Ensenada, Baja California (CICESE).
Sheriff, R.E., Geldart, L.P., 1995. Exploration Seismology, 2nd ed. Cambridge University Press, Estados Unidos.
Stephenson, W.J., Louie, J.N., Pullammanappallil, S., Williams, R.A., Odum, J.K., 2005. Blind shear-wave velocity comparison of ReMi and MASW results with boreholes to 200 m in Santa Clara Valley: Implications for earthquake ground-motion assessment. Bull. Seismol. Soc. Am. 95, 2506–2516. https://doi.org/10.1785/0120040240.
Wilson, I.F., Rocha, V.S., 1955. Geology and Mineral Deposits of the Bole Copper District, Baja California, Mexico. U.S. Geological Survey Professional. Paper 273. 134 p.. .
Xia, J., Miller, R.D., Park, C.B., 1999. Estimation of near-surface shear-wave velocity by inversion of Rayleigh waves. Geophysics 64, 691–700.
Xia, J., Miller, R.D., Park, C.B., Hunter, J.A., Harris, J.B., 2000. Comparing shear-wave velocity profiles from MASW with Borehole Measurements Multichannel raw field data dispersion curve of Rayleigh wave shear-wave velocity profile. JEEG 5, 1–13.
Yilmaz, O., 2001. Seismic Data Analysis, 2nd ed. Society of Exploration Geophysicists, Tulsa, USA.
Zollo, A., Maercklin, N., Vassallo, M., Dello Iacono, D., Virieux, J., Gasparini, P., 2008. Seismic reflections reveal a massive melt layer feeding Campi Flegrei caldera. Geophys. Res. Lett. 35, 0–5. https://doi.org/10.1029/2008GL034242.